



Optimal suturing techniques in patch-bridging reconstruction for massive rotator cuff tears: A finite element analysis

Yuting Zhong^{a,b,c,d,e,1}, Chengxuan Yu^{a,1}, Sijia Feng^a, Han Gao^{a,b}, Luyi Sun^a, Yunxia Li^a,
Shiyi Chen^{a,**}, Jun Chen^{a,*}

^a Sports Medicine Institute of Fudan University, Department of Sports Medicine, Huashan Hospital, Fudan University, Shanghai, 200040, PR China

^b Department of Orthopedic Surgery, The Second Affiliated Hospital, Zhejiang University School of Medicine, Hangzhou, Zhejiang, PR China

^c Orthopedics Research Institute of Zhejiang University, Hangzhou, Zhejiang Province, PR China

^d Key Laboratory of Motor System Disease Research and Precision Therapy of Zhejiang Province, Hangzhou, Zhejiang Province, PR China

^e Clinical Research Center of Motor System Disease of Zhejiang Province, PR China

ARTICLE INFO

Keywords:

Bridging
Finite element analysis
Massive rotator cuff tear
Patch
Suturing

ABSTRACT

Purpose: To use a finite element method to construct a patch-bridge repair model for massive rotator cuff tears (MRCTs) and investigate the effects of different suture methods and knot numbers on postoperative biomechanics.

Methods: A finite element model based on intact glenohumeral joint data was used for a biomechanical study. A full-thickness defect and retraction model of the supraspinatus tendon simulated MRCTs. Patch, suture, and anchor models were constructed, and the Marlow method was used to assign the material properties. Three suturing models were established: 1-knot simple, 1-knot mattress, and 2-knot mattress. The ultimate failure load, failure mode, stress distribution of each structure, and other biomechanical results of the different models were calculated and compared.

Results: The ultimate failure load of the 1-knot mattress suture (71.3 N) was 5.6 % greater than that of the 1-knot simple suture (67.5 N), while that (81.5 N) of the 2-knot mattress was 14.3 % greater than that of the 1-knot mattress. The stress distribution on the patch and supraspinatus tendon was concentrated on suture perforation. Failure of the bridging reconstruction mainly occurred at the suture perforation of the patch, and the damage forms included cutting-through and isthmus pull-out.

Conclusion: A finite element model for the patch-bridging reconstruction of MRCTs was established, and patch-bridging restored the mechanical integrity of the rotator cuff. The 2-knot mattress suture was optimal for patch-bridging reconstruction of MRCTs.

1. Introduction

A rotator cuff tear (RCT) is one of the most common causes of shoulder pain and dysfunction, accounting for approximately 40 % of all shoulder pain cases.¹ A massive rotator cuff tears (MRCTs) is defined when imaging or intraoperative findings show tendon retraction to the glenoid in the coronal or axial planes, or when 67 % or more of the greater tuberosity is exposed in the sagittal plane.² MRCTs are the most severe type of RCT, accounting for approximately 40 % of all rotator cuff

tears.³ Treatment of MRCTs has become challenging for surgeons as these severe injuries are accompanied by a high postoperative failure rate of 17.6%–94 %.^{4–7} Specifically, large cuff tears and MRCTs cannot be repaired by directly suturing the tendon back to the original attachment point. Even if repair is completed, excessive suture tension can lead to poor healing or retears.³

Many new surgical methods and repair materials have been developed and used clinically, such as rotator cuff-enhanced patch augmentation⁸ and patch-bridging reconstruction.⁹ Rotator-cuff patches are

* Corresponding author. Sports Medicine Institute of Fudan University, Department of Sports Medicine, Huashan Hospital, Fudan University, No. 12 Wulumuqi Zhong Road, Shanghai, 200040, PR China.

** Corresponding author. Sports Medicine Institute of Fudan University, Department of Sports Medicine, Huashan Hospital, Fudan University, No. 12 Wulumuqi Zhong Road, Shanghai, 200040, PR China.

E-mail addresses: shiyi_chen@fudan.edu.cn (S. Chen), biochenjun@fudan.edu.cn (J. Chen).

¹ Y. Zhong and C. Yu contributed equally to this work.

<https://doi.org/10.1016/j.asmart.2024.10.002>

Received 31 May 2024; Received in revised form 24 September 2024; Accepted 30 October 2024

2214-6873/© 2024 Asia Pacific Knee, Arthroscopy and Sports Medicine Society. Published by Elsevier (Singapore) Pte Ltd. This is an open access article under the CC BY-NC-ND license (<http://creativecommons.org/licenses/by-nc-nd/4.0/>).

specialized implants designed to provide specific shapes and mechanical strength. Patch augmentation is used to reinforce degenerated tendons or in cases of severe muscle atrophy, allowing for a low-tension repair.¹⁰ Patch-bridging reconstruction is for large tears where direct suturing would cause excessive tension, using a patch to connect the torn tendon to the humerus and reduce tension.¹¹ However, even with the successful use of rotator cuff patches in augmentation or bridging surgery for full-thickness rotator cuff tears, retears may still occur postoperatively, with a retear rate of approximately 2%–100%.¹² Meanwhile, higher mechanical requirements are needed for the patch^{13,14} in bridging repair compared to that in augmentation repair. Therefore, exploring the biomechanical changes of the rotator cuff patch in bridging repair surgery is crucial.

Finite element analysis (FEA) is a computer simulation technique

used in biomechanics that can yield multiple mechanical results under specific conditions through simulation and analysis. In recent years, with the development of medical imaging and computer processing power, FEA has more accurately simulated the geometric morphology of human tissue structures and obtained local mechanical data at different time points and positions in the dynamic process of testing.¹⁵ Currently, there is no related finite element (FE) simulation or analysis of large or massive full-thickness rotator cuff tears repaired using patch-bridging reconstruction. Thus, FEA can be used to explore the biomechanical changes in different structures after patch-bridging reconstruction for full-thickness rotator cuff tears.

In this study, FE techniques were used to build a full-thickness rotator cuff tear condition based on an FE model of a normal rotator cuff. The tear was then repaired using a bridging technique that was clinically

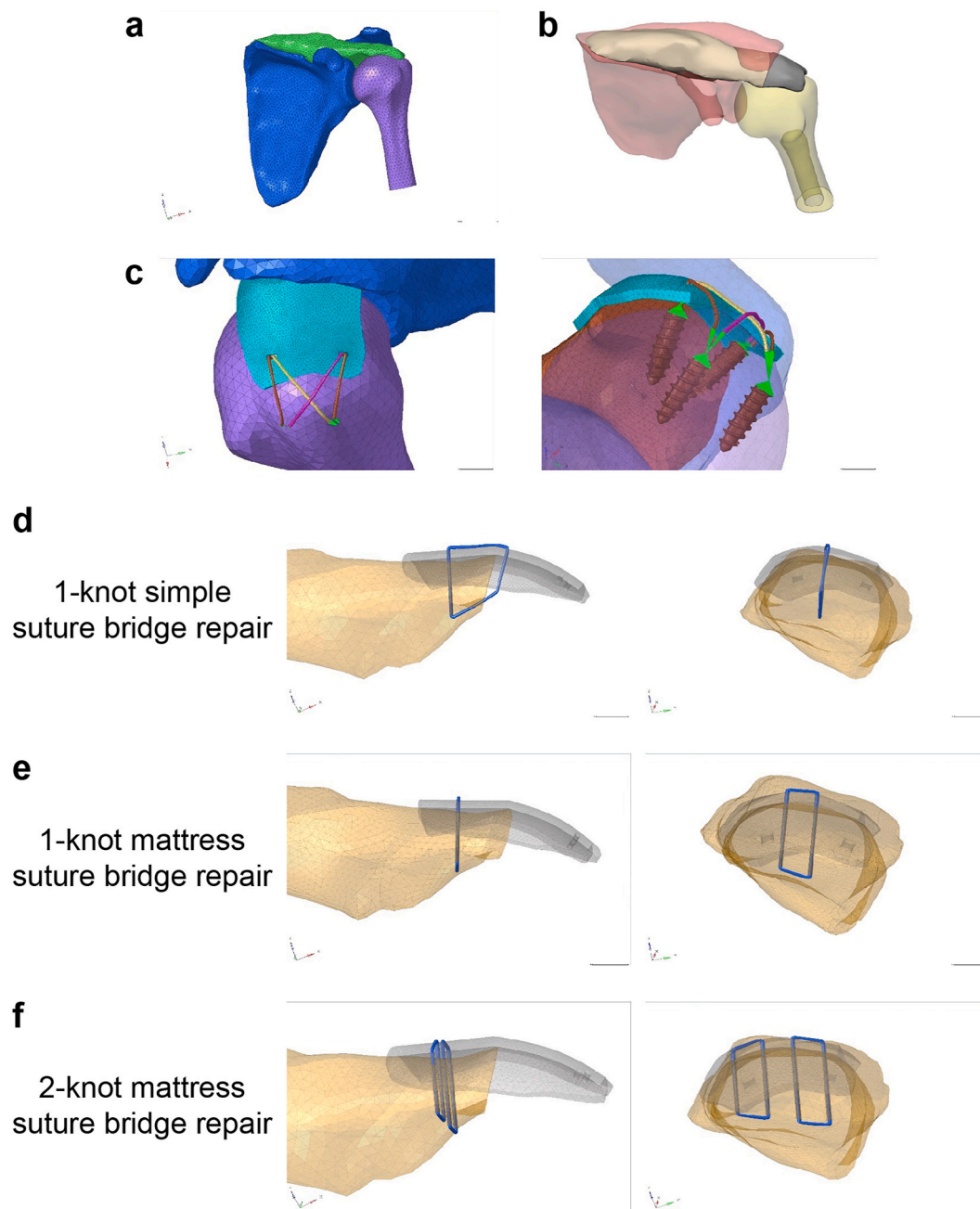


Fig. 1. Construction of the finite element model of full-thickness rotator cuff tears with different suture patterns. a) Mesh model of the bony and supraspinatus structures of the shoulder joint. b) Simulation of full-thickness rotator cuff tears with tendon retraction. c) Fixation of the patch on the humerus. d) Simulations of 1-knot simple suture bridge repair. e) Simulations of 1-knot mattress suture bridge repair. f) Simulations of 2-knot mattress suture bridge repair.

used while constructing different conditions with varying numbers and types of sutures. Each condition was tested and analyzed to investigate the effect of different patch-bridging sutures on the biomechanics of each structure in order to provide a reference for optimizing surgical procedures and improving the design of rotator cuff patches.

2. Methods

2.1. Development of the shoulder three-dimensional FE model

All procedures of this study were performed in compliance with relevant laws and institutional guidelines. The study was approved by the Health Sciences Institutional Review Board of Huashan hospital with informed consent obtained from the volunteer (KY2019-410, approved on August 28, 2019). The volunteer model was a 26-year-old male with no history of shoulder injuries or conditions, such as pain, dislocation, or fractures, and no abnormalities found on imaging examinations.^{16,17} The volunteer was scanned using a high-resolution computed tomography (CT) scanner with 1.5-mm slices and a magnetic resonance imaging (MRI) scanner with 1.0-mm slices. During both CT and MRI scanning, the shoulder was in a neutral position on the side of the body, and the body was in supine.

CT-Digital Imaging and Communications in Medicine (DICOM) and MRI-DICOM data were imported into the Mimics 10.0 (Materialise, Leuven, Belgium) software. The structures of the clavicle, scapula, humerus, and supraspinatus muscles were simulated based on bony structures in the Mimics software. Data from the FE shoulder model were saved as a stereolithography file for future transfer. Smoothing processing and solid construction were completed using Geomagic 9.0 (3D Systems, San Diego, CA), and the structures of the normal shoulder joint were further reassembled and meshed using HyperMesh 11.0 (Altair Engineering Inc., Troy, MI, USA).¹⁸ The FE mesh of the entire structure comprised C3D4 elements with an average edge length of 1 mm. The cortical bone of the scapula was 1.0-mm thick. For the connection between the supraspinatus tendon and the cortical bone of the humerus at the scapular stop point, a specific tolerance was set and bound using the Tie method, which allowed for the transfer of stress and strain parameters between the two meshes. The FE model is presented in Fig. 1a.

2.2. Design of the full-thickness rotator cuff tears with tendon retraction

Because the supraspinatus tendon is the most common site of rotator cuff tears in clinical practice,¹⁹ a full-thickness supraspinatus tear with a tendon retraction model was used to simulate rotator cuff tears. In HyperMesh, a 25-mm tendon defect was created on the supraspinatus tendon at its humeral attachment using a cutting tool (Fig. 1b).

2.3. Simulation of different suture patterns for suture-bridge repair with patch

Referring to the common patch morphology,²⁰ the design of the rotator cuff patch in this study was based on the shape of the side of the tendon stump. A smooth surface was created in the HyperMesh to connect the tendon stump to the attachment of the humeral tendon, and the surface was partially covered over the tendon stump at a thickness of 2 mm.²¹ A suitable hole was created at the appropriate suture location on both sides of the patch to allow the suture to pass through.

The suture-bridge procedure was performed by suturing the patch to the tendon stump at the tendon end, inserting a wire anchor on the humeral side, and passing the inner row of anchor wires through the patch to secure it to the lateral aspect of the greater tuberosity. The patch was fixed to the side of the humeral head with suture anchors.²² Two anchors (4.5 mm × 14 mm, Arthrex) were implanted 45° to the horizontal plane at the area of the supraspinatus lateral tendon attachment and at the lateral side of the humeral greater tubercle. A 2#

Fiberwire suture (Arthrex) with a 1-mm diameter suture was used for transosseous equivalent fixation at the greater tuberosity of the humerus.²³ The fixation was performed using a multipoint constraint (MPC) coupling restraint with anchor nails (Fig. 1c). The patches and tendon stumps were sutured using different patterns.

In the experiment, the following three different suture patterns were constructed and compared: 1-knot simple suture bridge repair, 1-knot mattress suture bridge repair, and 2-knot mattress suture bridge repair (Fig. 1d–f, respectively).

2.4. Material properties

For different anatomical structures, the FE models were assigned different material properties. To investigate the differences between different sutures, the bony structure and anchors were set as rigid bodies, and the tendon, sutures, and patch were set as destructible deformed.^{15,24} To investigate the form of damage, the patch was defined as having the same mechanical properties as the tendon. The material properties of each part of the shoulder joint structure, surgical anchors, and sutures are summarized in Table 1.

According to the biomechanical data of the rabbit rotator cuff tendon in the uniaxial tensile test, the force–displacement curve of the tendon was converted into an engineering stress–strain curve to simulate the biomechanical characteristics of the human supraspinatus tendon in the FE model. To define the material properties of the FEA, the test data were input into the ABAQUS software, and the material model was fitted with the Marlow model (Fig. 2). To further verify the effectiveness of the material model and program, an analysis model similar to the test was established using ABAQUS 6.10. A cuboid (27.2 mm × 5 mm × 1 mm) was established for the uniaxial tensile simulation test, and a force–displacement curve was obtained. To verify the accuracy of the material properties, the curve calculated from the simulation test was compared with the average force–displacement curve obtained from the experimental test. The two curves overlapped significantly, indicating that the fitting results of the tendon material properties were accurate and could reflect the actual situation, which could be used for subsequent analysis. Combined with the VUSDFLD subroutine in the ABAQUS, a custom program (SI Fig. 1) was written to specify that the element failure would be deleted at a specific stress (defined as the engineering stress corresponding to the maximum tensile test in this study).

Based on data from FiberWire in previous biomechanical studies,²⁵ inverse force–displacement data extraction was performed using the Origin software, and the Marlow model was used to obtain the material properties of the suture.

2.5. Boundary conditions

In this study, both the humerus and scapula were set as rigid bodies, and all degrees of freedom were fixed at the rigid-body control points at the acromion and humeral stem. At the muscle of the tendon stump, a distribution coupling constraint was established, and displacement was applied at the neutral point to simulate the relative slip between the muscle tuberosities during muscle contraction. General, internal, and self-contact of the outer surface were added between all parts, and the method used was hard contact. Separation was allowed after contact, and the tangential friction coefficient was set to 0.1. The suture anchors adopted the embedding setting and the suture was connected to the anchor through the MPC. Additionally, Abaqus 6.12–1 was used as the finite element solver, and large deformation (NLgeom) was enabled. The Newton-Raphson method was employed to solve the nonlinear equilibrium equations, with iterative controls adjusted to improve convergence, including the maximum computation steps and minimum step size.

Table 1
Material properties of the each part of the finite element model.

Structure		Young modulus (MPa)	Poisson ratio	Element type	Elements	Nodes
Cortical bone of the humerus		13,400	0.3	C3D4	3476	1729
Cancellous bone of the humerus		2000	0.26	C3D4	6679	4516
Cortical bone of the scapula		9000	0.3	C3D4	4026	2831
Cancellous bone of the scapula		2000	0.2	C3D4	17,439	9753
Anchor		3500	0.3	C3D4	234,356	57,792
Supraspinatus muscle	1-knot simple suture bridge repair	Marlow model	/	C3D4	59,077	12,188
	1-knot mattress suture bridge repair				60,688	12,782
	2-knot mattress suture bridge repair				68,561	14,184
Patch	1-knot simple suture bridge repair	Marlow model	/	C3D4	116,270	26,398
	1-knot mattress suture bridge repair				57,767	13,890
	2-knot mattress suture bridge repair				27,302	6988
Suture	1-knot simple suture bridge repair	Marlow model	/	C3D8	3408	4775
	1-knot mattress suture bridge repair				4144	5702
	2-knot mattress suture bridge repair				8288	11,404

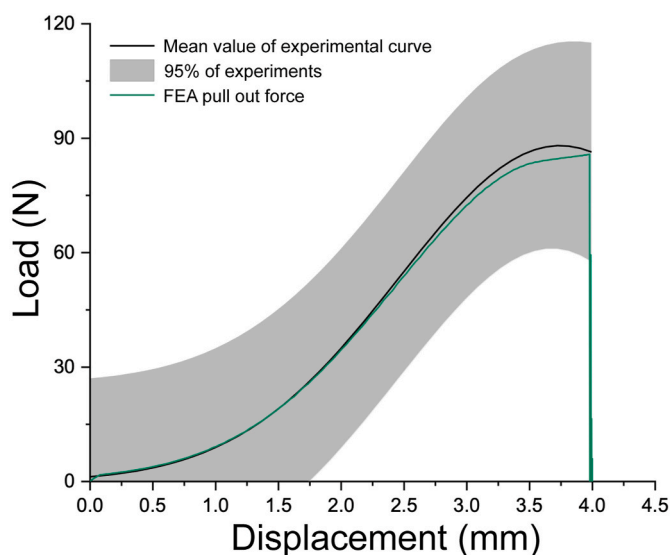


Fig. 2. Force–displacement curves of the supraspinatus tendon. The green line is the curve obtained from the finite element simulation test, and the black line is the average force–displacement curve of the experimental test. (For interpretation of the references to colour in this figure legend, the reader is referred to the Web version of this article.)

3. Results

3.1. Comparison of biomechanical analysis across models

In the simulation of the 1-knot simple suture bridge repair, with an increase in the force, the lateral patch structure of the inner needle hole first began to sustain minor damage at approximately 67 N, and the ultimate failure load was 67.5 N (Fig. 3a). When the muscle further contracted, the suture gradually tightened, thereby creating a cutting effect along the direction of the tendon fibers that led to patch destruction. The cutting of the patch firstly occurred on the medial side of the patch, and the “Z-shaped” oblique tear in the patch was formed on the upper surface of the patch, the lateral side of the inner suture point and the medial side of the inner needle hole on the lower surface of the patch. Simultaneously, the angle between the sutures on both sides of the inner needle holes gradually increased. Finally, the patch material between the two sutures on the patch was damaged, which led to patch failure. At this point, the humeral suture of the patch was partially damaged.

When the 1-knot mattress suture bridge repair was used, the force of the bridge repair system gradually increased with muscle contraction, and the suture was deformed (Fig. 3b). At approximately 71.3 N, the

lateral needle hole on the upper surface of the tendon was slightly damaged, and the ultimate failure load was 71.3 N. When the muscle further contracted, the relative displacement between the patch and tendon continued to increase. Damage to the needle hole on the upper surface of the tendon further increased, and the structure of the suture crossing the lower surface of the tendon and the upper surface of the patch also began to be damaged. The patch material between the needle holes was strangled and completely protruded from the patch. The suture on the tendon side did not strangle the tendon tissue on the lower surface, and only part of the tissue near the needle hole was destroyed. The patch also demonstrated a partial microdisruption of the needle hole in the lateral humeral suture.

In the model of the 2-knot mattress suture bridge repair, with the increase of the force, at approximately 79 N, the lateral side of the needle hole on the upper surface of the tendon was the first to be damaged, and the suture was stretched and deformed (Fig. 3c). When the muscle further contracted, the relative displacement between the patch and tendon increased continuously, and the needle hole on the inferior surface of the tendon and the needle hole on the patch began to fail at approximately 81 N. The ultimate failure load was 81.5 N. As the deformation of the patch increased, the suture on the anchor of the humeral side began to cut the patch along the tendon direction. Finally, the patch was destroyed, and the suture on the humeral side completely prolapsed from the patch.

In conclusion, the FEA experiment was used to test the displacement of the main node and the force of the entire system during muscle contraction. The ultimate failure loads and failure positions for each working condition are listed in Table 2. The ultimate failure load of the 1-mattress suture bridge repair was slightly larger than that of the 1-knot simple suture bridge repair by approximately 5.6 %, while that of the 2-knot mattress suture bridge repair was approximately 14.3 % higher than that of the 1-knot mattress suture bridge repair.

3.2. Comparison of the stress distribution across patches

As presented in Fig. 4a–c, the stress of each part of the patch was concentrated on the needle hole of the patch under the ultimate failure load in each working condition, and the stress of the remaining parts was small. After the local stress of the suture exceeded the set maximum value, the corresponding FE on the patch was considered invalid and deleted, which was consistent with the general appearance of the patch being cut and damaged by the suture.

3.3. Comparison of the stress distribution across tendon stumps

When the ultimate failure load was reached, the stress on each part of the tendon stump was mainly concentrated on the patch-side needle hole of the tendon, and the rest of the tendon-suture contact part and the internal stress of the tendon were relatively small (Fig. 5a–c). Under the

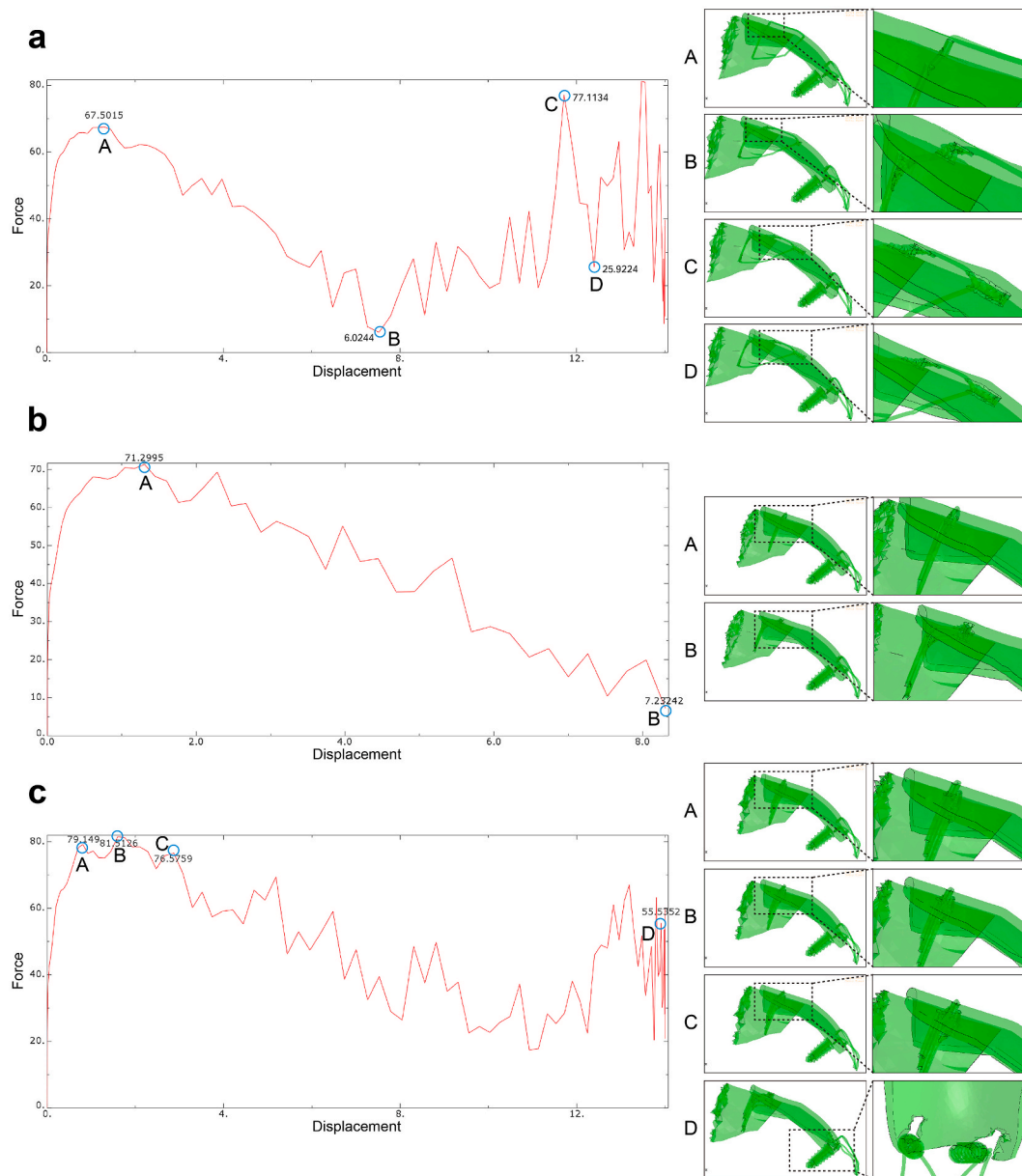


Fig. 3. Force–displacement curves and failure modes of each suture pattern. a) Analyses of 1-knot simple suture bridge repair. b) Analyses of 1-knot mattress suture bridge repair. c) Analyses of 2-knot mattress suture bridge repair.

Table 2
Ultimate failure load and failure position of bridge repair with different suture patterns.

Suture patterns	Ultimate failure load (N)	Failure position
1-knot simple suture bridge repair	67.5	Tendon stump side of the patch
1-knot mattress suture bridge repair	71.3	Tendon stump side of the patch
2-knot mattress suture bridge repair	81.5	Humerus and suture anchors' side of the patch

condition of 2-mattress suture bridge repair, the suture passed through the tendon four times, and the stress was mainly concentrated on the two outer needle holes (Fig. 5c).

4. Discussion

In this study, a normal shoulder joint FE model was constructed, followed by a model of a full-thickness supraspinatus tendon tear with retraction. Based on this, patch-bridge reconstructions with different types and numbers of sutures were simulated, and the maximum failure load, stress distribution of each model under different conditions were compared. The results demonstrated that the patch first failed at the suture where the thread passed through the patch, and the maximum ultimate load of the patch was achieved with the 2-knot mattress suture bridge repair.

Each of the three suturing methods evaluated in this study—1-knot simple, 1-knot mattress, and 2-knot mattress—has its own advantages and limitations. The 1-knot simple suture is technically easier to perform and less time-consuming, but it provides lower ultimate failure load, making it less suitable for high-stress repairs. The 1-knot mattress suture offers a balance between ease of use and mechanical strength, but its failure load is still lower compared to more complex methods. The 2-

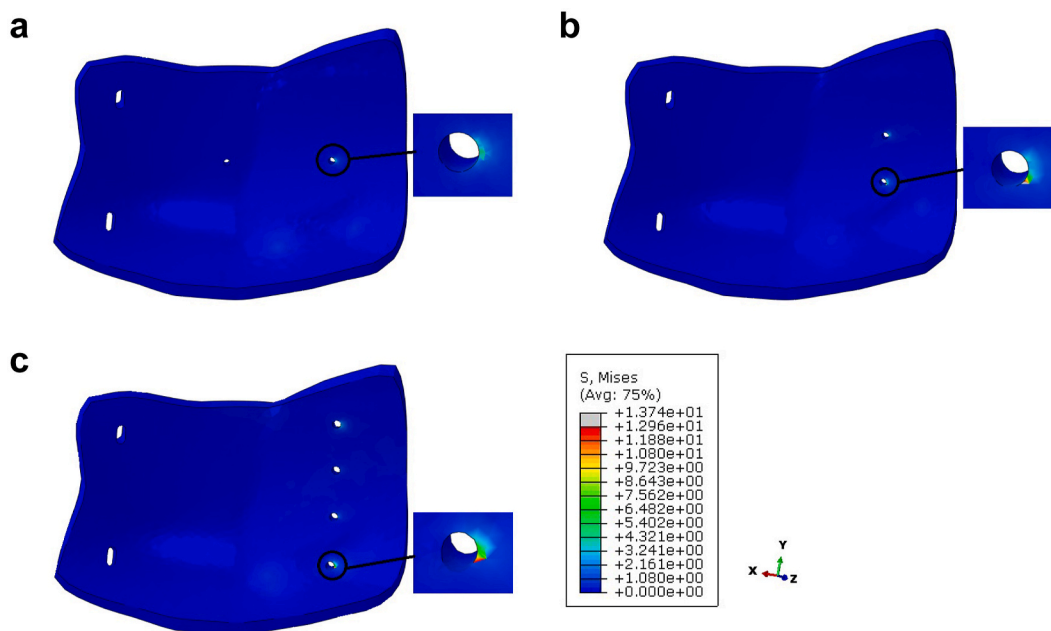


Fig. 4. Contour plots of the stress of the patch. a) Stress distribution patterns of the patch in the 1-knot simple suture bridge repair. b) Stress distribution patterns of the patch in the 1-knot mattress suture bridge repair. c) Stress distribution patterns of the patch in the 2-knot mattress suture bridge repair.

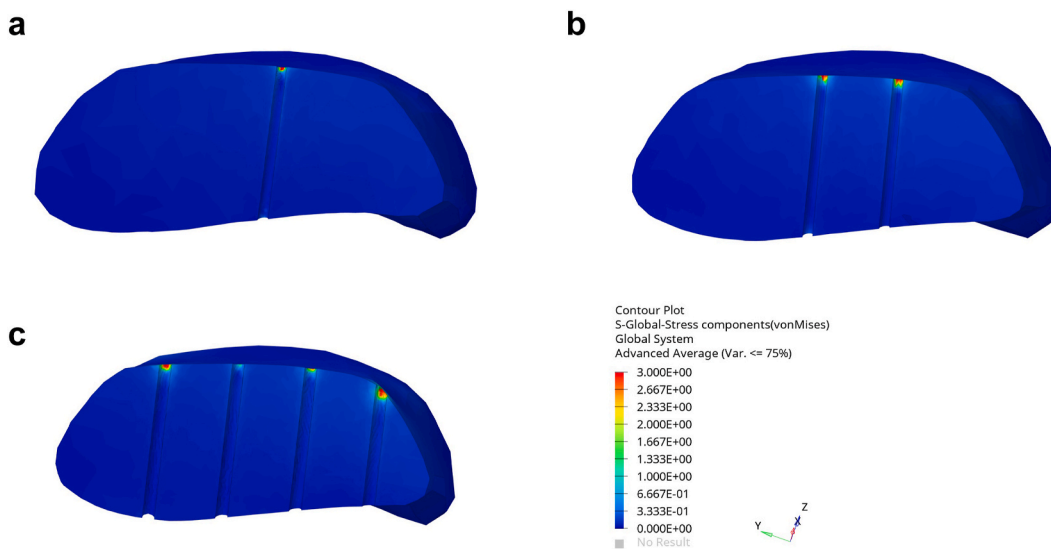


Fig. 5. Contour plots of the stress of the tendon stump. a) Stress distribution patterns of the tendon stump in the 1-knot simple suture bridge repair. b) Stress distribution patterns of the tendon stump in the 1-knot mattress suture bridge repair. c) Stress distribution patterns of the tendon stump in the 2-knot mattress suture bridge repair.

knot mattress suture, while more technically demanding, provided the highest ultimate failure load and better stress distribution, making it the most effective option for restoring mechanical integrity in patch-bridging repairs. Future studies could further explore how these suturing techniques perform under different clinical conditions and how they affect long-term healing outcomes.

The type and number of sutures influenced the maximum load on the rotator cuff and patch. The tendon end of the rotator cuff can be sutured in many ways, such as simple, mattress, Mason–Allen, and Kessler sutures. This study compared common and simple methods of using simple and mattress sutures. Gerber et al. tested the maximum load of the rotator cuff using different suture techniques in a sheep infraspinatus specimen and reported that the maximum load of the 2-knot mattress suture was significantly higher than that of simple sutures.²⁶

Additionally, as the number of sutures increased, the maximum load did not increase proportionally, which was similar to the FEA results.

Previous studies have reported significant differences in the biomechanical outcomes of bridging patch repair, which may be influenced by the testing methods, patch size, and patch type.^{27–29} Most previous studies only reported on parameters such as ultimate load, stiffness, and elastic modulus; however, both patches and tendons are viscoelastic materials, and the actual stress–strain curves are not completely linear, particularly in the region of plastic deformation beyond the elastic limit, where tearing may occur,³⁰ thus making it difficult to directly use published data for FEA.

In this study, the Marlow constitutive model was used to fit the measured tendon force–displacement curve to better explore the failure modes of the bridged patch after suture repair. The material parameters

were adjusted such that the stress and strain were more closely aligned with the actual situation. The patch parameters were set consistent with the tendon to ensure that the patch failed before the residual tendon. In previous studies, patch failure modes were divided into two types²⁸: suture pull-out from the patch material and patch tearing while the suture remained on the patch. The former is further divided into three forms as follows: isthmus pull-out, side pull-out, and end pull-out, with the isthmus pull-out being the most common. This study demonstrated that as the muscle contraction displacement increased, the main failure mode of the patch was parallel cutting in the direction of the tendon when using simple sutures and button-like tear-out or the so-called isthmus pull-out in the direction perpendicular to the tendon when using mattress sutures, which was consistent with the results of previous biomechanical studies.^{28,31} Meanwhile, the stress concentration and first failure position of the patch were both at the suture, whereas the stress in other parts was smaller, indicating that increasing the mechanical strength of the contact site between the suture and patch should be especially considered when designing a bridged shoulder patch. Currently, common reinforcement methods include local thickening, use of composite materials, and special weaving. The effectiveness of the patch reinforcement design can be evaluated by testing a specific patch and assigning the patch material properties to the FE model.

As biomechanical studies have shown, suture techniques play a critical role in the success of rotator cuff repairs. In previous study, the ultimate load of the single simple suture (47.1 ± 23.0 N) and the 1-knot mattress suture (67.1 ± 27.7 N) was evaluated based on the biomechanical test.³² These failure loads and failure modes are consistent with our FEA results, emphasizing the importance of analyzing optimal suture techniques to improve tendon stability and reduce the risk of postoperative retears. Therefore, careful consideration of suture methods is crucial for optimizing surgical outcomes and enhancing patient recovery, and the reliability of the FEA results in this study supports this conclusion.

It should be noted that the maximum load analyzed by FEA in this study was only simulated data immediately postoperatively, and the subsequent in vivo healing process had a significant impact on the biomechanics. In a review, Sunwoo has reported that after completing bridge patch repair, the maximum load and stiffness of the reconstructed rotator cuff increased with time and the healing process.²⁷ Kimura used PTFE patches for bridge patch repair to compare them with the dog infraspinatus bridge patch repair model, and the maximum load 12 weeks postoperatively was significantly higher than that immediately postoperatively (12 weeks vs. time 0, 307 N vs. 61 N).³³ Adams obtained similar results using acellular dermal matrix patches (12 weeks vs. time 0, 539 N vs. 63 N).³⁴ However, the increase in mechanical strength of the small intestine submucosa patches was smaller than that of the other patches (6 months vs. time 0, 85 N vs. 31 N), and was significantly lower than that of the normal tendons.³⁵ Therefore, the FEA mainly provides a reference for patch design and surgical operations, and specific patch and suture methods need to be further verified in vivo.

The FE model constructed in this study has several advantages. First, unlike previous FEAs that often used linear structures to simulate muscles and assigned a single elastic modulus value, this study not only constructed a three-dimensional solid structure of the supraspinatus muscle, but also used the Marlow constitutive model to fit the force–displacement curve of the tendon and suture to provide different elastic moduli to the tendon under different stretching displacements, which is closer to the actual biomechanical properties of the tissue and has a higher degree of simulation. Second, the suture conditions were based on real clinical surgical procedures, and the suture parameters were based on the products used in the clinic. Detailed simulation calculations and analyses of different surgical sutures provide reference values for optimizing the surgical approach. Finally, this model can be reused multiple times, and by simply modifying the parameters, it can simulate and test the mechanical properties of patch materials with different material properties under different suture conditions. Moreover, it can

provide a reference for patch design and a means of simulated testing for patch-finished products.

This study had several limitations. First, the model constructed in this study was based on only one healthy volunteer, which could not avoid the influence of individual differences. Second, rabbit tendons were used to simulate human tendon parameters. Differences in the material properties of tendons across species or the type of suturing techniques employed may contribute to the variation in biomechanical outcomes. In future research, tendons corresponding to age and disease should be collected and tested, and the influence of sex should be considered to obtain more accurate analysis results. Furthermore, this study only analyzed the failure mode under direct tension and did not consider the fatigue failure mode under low-load cyclic loading. In future studies, the fatigue life of different products, surgical procedures and other variations in experimental setup should be analyzed according to postoperative activity levels in humans. While other repair techniques and factors could be explored in clinical practice, this study focused on using FEA technology to provide an in-depth analysis of stress distribution and simulated failure across three patch-bridging reconstruction models for rotator cuff repair. This analysis offers valuable insights that could help inform the selection of suturing techniques in clinical settings.

5. Conclusion

An FE model for the patch bridging reconstruction of MRCTs was established, and it was verified that patch bridging could restore the mechanical integrity of the rotator cuff. Among the conditions investigated in this study, the 2-knot mattress suture was optimal for patch-bridging reconstruction of MRCTs. This study provides a theoretical basis for optimizing RCT treatments of rotator cuff tears using patch grafts.

Acknowledgments

The authors acknowledge Dr. Chen Bo and Dr. Cai Fangzhou, Ruijin Hospital, Shanghai Jiaotong University School of Medicine, for their assistance in modelling methods. This work was supported by National Key R&D Program of China (2021YFA1201303), Clinical Research Plan of SHDC (SHDC2022CRT021), National Natural Science Foundation of China (No. 82172511).

Appendix A. Supplementary data

Supplementary data to this article can be found online at <https://doi.org/10.1016/j.asmart.2024.10.002>.

References

- Linsell L, Dawson J, Zondervan K, et al. Prevalence and incidence of adults consulting for shoulder conditions in UK primary care; patterns of diagnosis and referral. *Rheumatology*. 2006;45:215–221.
- Schumaier A, Kovacevic D, Schmidt C, et al. Defining massive rotator cuff tears: a Delphi consensus study. *J Shoulder Elbow Surg*. 2020;29:674–680.
- Godeneche A, Freychet B, Lanzetti RM, Clechet J, Carrillon Y, Saffarini M. Should massive rotator cuff tears be reconstructed even when only partially repairable? *Knee Surg Sports Traumatol Arthrosc*. 2017;25:2164–2173.
- Galatz LM, Ball CM, Teefey SA, Middleton WD, Yamaguchi K. The outcome and repair integrity of completely arthroscopically repaired large and massive rotator cuff tears. *J Bone Joint Surg Am*. 2004;86:219–224.
- Sugaya H, Maeda K, Matsuki K, Moriishi J. Repair integrity and functional outcome after arthroscopic double-row rotator cuff repair. A prospective outcome study. *J Bone Joint Surg Am*. 2007;89:953–960.
- Park J-Y, Siti HT, Keum J-S, Moon S-G, Oh K-S. Does an arthroscopic suture bridge technique maintain repair integrity?: a serial evaluation by ultrasonography. *Clin Orthop Relat Res*. 2010;468:1578–1587.
- Paxton ES, Teefey SA, Dahiya N, Keener JD, Yamaguchi K, Galatz LM. Clinical and radiographic outcomes of failed repairs of large or massive rotator cuff tears: minimum ten-year follow-up. *J Bone Joint Surg Am*. 2013;95:627–632.

8. Ferguson DP, Lewington MR, Smith TD, Wong IH. Graft utilization in the augmentation of large-to-massive rotator cuff repairs: a systematic review. *Am J Sports Med.* 2016;44:2984–2992.
9. Lewington MR, Ferguson DP, Smith TD, Burks R, Coady C, Wong IH. Graft utilization in the bridging reconstruction of irreparable rotator cuff tears: a systematic review. *Am J Sports Med.* 2017;45:3149–3157.
10. Ferguson DP, Lewington MR, Smith TD, Wong IH. Graft utilization in the augmentation of large-to-massive rotator cuff repairs: a systematic review. *Am J Sports Med.* 2016;44:2984–2992.
11. Lewington MR, Ferguson DP, Smith TD, Burks R, Coady C, Wong IH-B. Graft utilization in the bridging reconstruction of irreparable rotator cuff tears: a systematic review. *Am J Sports Med.* 2017;45:3149–3157.
12. Baldwin M, Nagra NS, Greenall G, et al. Use of implantable meshes for augmented rotator cuff repair: a systematic review and meta-analysis. *BMJ Open.* 2020;10, e039552.
13. Badhe SP, Lawrence TM, Smith F, Lunn P. An assessment of porcine dermal xenograft as an augmentation graft in the treatment of extensive rotator cuff tears. *J Shoulder Elbow Surg.* 2008;17:S35–S39.
14. Soler JA, Gidwani S, Curtis MJ. Early complications from the use of porcine dermal collagen implants (Permacol) as bridging constructs in the repair of massive rotator cuff tears. A report of 4 cases. *Acta Orthop Belg.* 2007;73:432–436.
15. Redepenning DH, Ludewig PM, Looft JM. Finite element analysis of the rotator cuff: a systematic review. *Clin Biomech.* 2020;71:73–85.
16. Yang Z, Xu G, Yang J, Li Z. Effect of different loads on the shoulder in abduction postures: a finite element analysis. *Sci Rep.* 2023;13:9490.
17. Yang Z, Xu G, Yang J, Lin X. Finite element study of the biomechanical effects on the rotator cuff under load. *Front Bioeng Biotechnol.* 2023;11, 1193376.
18. Duprey S, Bruyere K, Verriest JP. Human shoulder response to side impacts: a finite element study. *Comput Methods Biomech Biomed Eng.* 2007;10:361–370.
19. Sambandam SN, Khanna V, Gul A, Mounasamy V. Rotator cuff tears: an evidence based approach. *World J Orthoped.* 2015;6:902–918.
20. Bailey JR, Kim C, Alentorn-Geli E, et al. Rotator cuff matrix augmentation and interposition: a systematic review and meta-analysis. *Am J Sports Med.* 2019;47:1496–1506.
21. Seker V, Hackett L, Lam PH, Murrell GAC. Evaluating the outcomes of rotator cuff repairs with polytetrafluoroethylene patches for massive and irreparable rotator cuff tears with a minimum 2-year follow-up. *Am J Sports Med.* 2018;46:3155–3164.
22. Nho SJ, Delos D, Yadav H, et al. Biomechanical and biologic augmentation for the treatment of massive rotator cuff tears. *Am J Sports Med.* 2010;38:619–629.
23. Quental C, Reis J, Folgado J, Monteiro J, Sarmento M. Comparison of 3 supraspinatus tendon repair techniques - a 3D computational finite element analysis. *Comput Methods Biomech Biomed Eng.* 2020;23:1387–1394.
24. Zheng M, Zou Z, Bartolo PJ, Peach C, Ren L. Finite element models of the human shoulder complex: a review of their clinical implications and modelling techniques. *Int J Numer Method Biomed Eng.* 2017;33.
25. Jhamb A, Goldberg J, Harper W, Butler A, Smitham P, Walsh W, eds. *String Theory: An Examination of the Properties of "High Strength" Suture Materials.* Annual Scientific Meeting of the Australian Orthopaedic Association; 2007.
26. Gerber C, Schneeberger AG, Beck M, Schlegel U. Mechanical strength of repairs of the rotator cuff. *J Bone Joint Surg Br.* 1994;76:371–380.
27. Sunwoo JY, Murrell GAC. Interposition graft repair of irreparable rotator cuff tears: a review of biomechanics and clinical outcomes. *J Am Acad Orthop Surg.* 2020;28: e829–e838.
28. Barber FA, Herbert MA, Coons DA. Tendon augmentation grafts: biomechanical failure loads and failure patterns. *Arthroscopy.* 2006;22:534–538.
29. McKeown A, Beattie RF, Murrell GA, Lam PH. Biomechanical comparison of expanded polytetrafluoroethylene (ePTFE) and PTFE interpositional patches and direct tendon-to-bone repair for massive rotator cuff tears in an ovine model. *Shoulder Elbow.* 2016;8:22–31.
30. Rawson SD, Margetts L, Wong JK, Cartmell SH. Sutured tendon repair; a multi-scale finite element model. *Biomech Model Mechanobiol.* 2015;14:123–133.
31. Ronquillo JC, Lam P, Murrell GA. Arthroscopic ePTFE patch repair for irreparable rotator cuff tears: part I surgical technique and biomechanical comparison of 2-suture techniques at the patch to tendon interface. *Tech Shoulder Elbow Surg.* 2013;14: 29–32.
32. Ponce BA, Hosemann CD, Raghava P, Tate JP, Eberhardt AW, Lafosse L. Biomechanical evaluation of 3 arthroscopic self-cinching stitches for shoulder arthroscopy: the lasso-loop, lasso-mattress, and double-cinch stitches. *Am J Sports Med.* 2011;39:188–194.
33. Kimura A, Aoki M, Fukushima S, Ishii S, Yamakoshi K. Reconstruction of a defect of the rotator cuff with polytetrafluoroethylene felt graft. Recovery of tensile strength and histocompatibility in an animal model. *J Bone Joint Surg Br.* 2003;85:282–287.
34. Adams JE, Zobitz ME, Reach Jr JS, An KN, Steinmann SP. Rotator cuff repair using an acellular dermal matrix graft: an in vivo study in a canine model. *Arthroscopy.* 2006;22:700–709.
35. DeJardin LM, Arnoczky SP, Ewers BJ, Haut RC, Clarke RB. Tissue-engineered rotator cuff tendon using porcine small intestine submucosa. Histologic and mechanical evaluation in dogs. *Am J Sports Med.* 2001;29:175–184.